© 2014. Published by The Company of Biologists Ltd | The Journal of Experimental Biology (2014) 217, 4372-4378 doi:10.1242/jeb.110296

RESEARCH ARTICLE

The mechanics of elastic loading and recoil in anuran jumping

Henry C. Astley* and Thomas J. Roberts

ABSTRACT

Many animals use catapult mechanisms to produce extremely rapid movements for escape or prey capture, resulting in power outputs far beyond the limits of muscle. In these catapults, muscle contraction loads elastic structures, which then recoil to release the stored energy extremely rapidly. Many arthropods employ anatomical 'catch mechanisms' to lock the joint in place during the loading period, which can then be released to allow joint motion via elastic recoil. Jumping vertebrates lack a clear anatomical catch, yet face the same requirement to load the elastic structure prior to movement. There are several potential mechanisms to allow loading of vertebrate elastic structures, including the gravitational load of the body, a variable mechanical advantage, and moments generated by the musculature of proximal joints. To test these hypothesized mechanisms, we collected simultaneous 3D kinematics via X-ray Reconstruction of Moving Morphology (XROMM) and single-foot forces during the jumps of three *Rana pipiens*. We calculated joint mechanical advantage, moment and power using inverse dynamics at the ankle, knee, hip and ilio-sacral joints. We found that the increasing proximal joint moments early in the jump allowed for high ankle muscle forces and elastic pre-loading, and the subsequent reduction in these moments allowed the ankle to extend using elastic recoil. Mechanical advantage also changed throughout the jump, with the muscle contracting against a poor mechanical advantage early in the jump during loading and a higher mechanical advantage late in the jump during recoil. These 'dynamic catch mechanisms' serve to resist joint motion during elastic loading, then allow it during elastic recoil, functioning as a catch mechanism based on the balance and orientation of forces throughout the limb rather than an anatomical catch.

KEY WORDS: Catch mechanism, Muscle, Frog, Catapult, Tendon

INTRODUCTION

Elastic energy storage is used by a wide variety of animals to produce movements that are faster and more powerful than muscle alone is capable of (Patek et al., 2011; Roberts and Azizi, 2011). Many animals employ 'catapult mechanisms', where contraction of a muscle acts to store energy in elastic structures prior to movement. Muscle initially actively shortens, stretching and storing energy in the elastic structure, after which the elastic structure recoils, rapidly releasing the stored energy and producing a high-power joint movement.

During the initial loading phase, the tension in the muscle and series elastic element will also exert a torque at the joint that, if unopposed, will produce joint movement rather than stretching the elastic structure. This poses a challenge to elastic energy storage systems, which require some method to resist the joint torque and allow stretching of the elastic structure. Inertia and gravitational loads can serve this purpose, delaying and slowing motion while the elastic element stretches (Galantis and Woledge, 2003; Roberts and Marsh, 2003). However, these mechanisms only allow for low-power catapult mechanisms (Galantis and Woledge, 2003), and many systems show much higher power outputs (Peplowski and Marsh, 1997; Patek et al., 2004; Burrows, 2006).

Arthropods frequently use anatomical 'catch mechanisms' to prevent joint movement and oppose the force of the muscle as the elastic element is loaded (Gronenberg, 1996). These anatomical catch mechanisms include exoskeletal latches (Heitler, 1974; Burrows, 2003; Patek et al., 2004) and changes in tendon leverage caused by a specialized muscle (Bennet-Clark and Lucey, 1967). In contrast, no anatomical catch mechanism has been located in vertebrates that utilize catapult mechanisms for jumping, although they also face the challenge of limiting joint movement during elastic loading. Anurans are perhaps the most well-studied group of vertebrate jumpers employing a catapult-like mechanism. No anatomical catch or latch has been identified in frogs, but direct measurements of muscle fiber length changes in the plantaris muscle of ranid frogs indicate that there is significant elastic pre-loading, that is, shortening of muscle against series elastic elements prior to movement (Astley and Roberts, 2012).

The goal of the present study was to determine how elastic pre-loading in frogs (*Rana pipiens* Schreber 1782) might occur in the absence of a physical catch mechanism. We focused on potential pre-loading in the plantaris muscle, an ankle extensor with a significant series-elastic tendon. Elastic pre-loading requires that the muscle in series with the elastic tendon develops high forces before motion of the ankle begins, because energy is stored in elastic structures when muscle force rises and released when it declines. In the absence of a physical catch, the force developed prior to motion can be approximated by a simple relationship between the muscle mechanical advantage and the ground reaction force (GRF):

$$\mathbf{F}_{\mathrm{m}} = \mathrm{GRF} \cdot R / r \,, \qquad (1)$$

where $\mathbf{F}_{\mathrm{m}}$ is the muscle force, R is the out-moment arm for this force and r is the in-moment or anatomical moment arm for the plantaris muscle (Fig. 1). From this equation it is clear that one way to develop high forces in the plantaris is to operate with a high value of R/r, i.e. with a ratio of moment arms that gives the plantaris muscle a poor mechanical advantage for force production against the body's center of mass. A previous modeling study showed that a poor mechanical advantage during elastic pre-loading, followed by an improving mechanical advantage to allow for elastic energy release, may allow for the high power outputs observed during a jump (Roberts and Marsh, 2003).

Eqn 1 indicates that high forces in the ankle musculature could also result from a high value of the GRF. In a static situation, the GRF is simply equal to one body weight (BW), and it is possible that body weight alone could be sufficient to allow for high plantaris forces prior to ankle motion. Previous modeling studies suggest that the magnitude of power amplification possible using this mechanism is limited (Galantis and Woledge, 2003; Roberts and Marsh, 2003).

Brown University, Department of Ecology and Evolutionary Biology, Providence, RI 02912, USA.

*Author for correspondence (henry.astley@physics.gatech.edu)

Received 30 June 2014; Accepted 27 October 2014

The Journal of Experimental Biology

The Journal of Experimental Biology (2014) doi:10.1242/jeb.110296

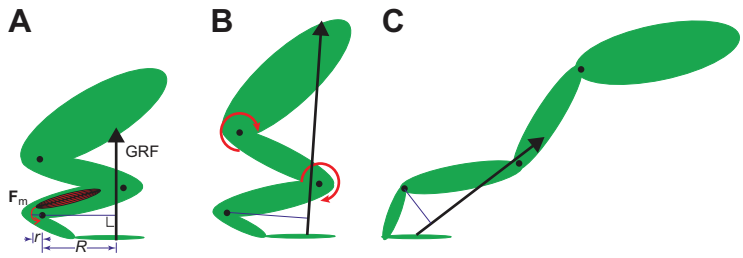

Fig. 1. Schematic diagram of hypothesized dynamic catch mechanisms. (A) Prior to joint motion, the force in the plantaris muscle ($\mathbf{F}_m$) is approximately equal to the product of the ground reaction force (GRF) and external moment arm (R) divided by the internal (muscle) moment arm (r), as given in Eqn 1 in the Introduction. Mechanisms that tend to increase $\mathbf{F}_m$ prior to joint movement will increase elastic pre-loading. In a gravitational catch mechanism, joint motion begins as soon as $\mathbf{F}_m$ begins to rise beyond the level needed to support body weight. (B) Extension moments of proximal joints and resultant acceleration of the body will increase GRF, possibly increasing $\mathbf{F}_m$ prior to ankle extension. (C) Variable mechanical advantage due to changes in external moment arm (R) during the jump may result in a poor mechanical advantage for $\mathbf{F}_m$ to resist motion during the loading phase, but a high mechanical advantage during recoil.

The magnitude of the GRF depends not only on gravity but also on inertial forces as the body is accelerated by the hindlimb musculature. If pre-loading of elastic elements at the ankle is to occur, by definition, before the onset of ankle motion, increases in GRF due to acceleration of the body would require motion (specifically, acceleration) at the knee or hip joints that precedes motion at the ankle. This suggests an alternative mechanism to facilitate elastic energy storage at the ankle, one not previously explored in simplified models of jumping (Roberts and Marsh, 2003). During jumping, early extension of more proximal joints could increase the GRF prior to ankle extension to allow for higher ankle muscle forces and elastic energy storage. Human jumpers employ a proximal-to-distal sequence of joint extensions, and it has been argued that this kinematic pattern allows for effective use of biarticular muscles and application of kinetic energy to the body center of mass (Bobbert and van Ingen Schenau, 1988). A proximal–distal sequence of joint extension in frogs might also aid in elastic energy pre-storage at the ankle by allowing for high ankle muscle forces prior to movement (Eqn 1).

We used inverse dynamics to investigate possible pre-loading of elastic energy at the ankle in frogs. Joint angles, moments and powers were calculated from a combination of single-foot forces measured via force plate and kinematics determined from X-ray reconstruction of moving morphology (Brainerd et al., 2010). We used the pattern of GRFs and joint dynamics to test for the three possible mechanisms for facilitating elastic pre-loading outlined above: (1) variable mechanical advantage; (2) gravitational loading during elastic energy storage; and (3) increased loading due to early extension of proximal joints. These mechanisms are not mutually exclusive but the contribution of each can be tested independently by the following predictions. If a variable mechanical advantage (r/R) contributes a catch-like mechanism, then the external moment arm (R) should be high early in the jump, and should decrease during the period of elastic recoil (muscle moment arm r is constant across ankle joint angle for the plantaris) (Astley and Roberts, 2012). If gravitational forces are sufficient to allow the majority of elastic loading, we predict that elastic recoil will occur close to the time the GRF begins to exceed 1 BW. Finally, if the action of proximal joints contributes to elastic pre-loading, then extension moments of the knee and hip must rise early in the jump, during the period of elastic loading, then decline during elastic recoil.

RESULTS

Performance

We captured synchronous X-ray video and force from three frogs; a total of eight jumps of varying orientation and magnitude remained after excluding jumps unsuitable for analysis (too far to the left/right, bad foot placement, etc.; Table 1). Jumps were sub-maximal (Table 1) but comparable to other laboratory studies of this species and congenerics (Emerson, 1978; Zug, 1978; Marsh, 1994; Lutz and Rome, 1996; Roberts and Marsh, 2003), and it has been demonstrated that significant elastic energy storage and tendon recoil occurs even during submaximal jumps in this species (Astley and Roberts, 2012). Figs 2–4 show data from the jump with the highest take-off velocity (Table 1, bottom row).

Joint kinematics and kinetics

All joints moved primarily via rotation about the flexion–extension axis, with much smaller and more variable motions in other degrees of freedom (Fig. 3B; supplementary material Fig. S1). Iliosacral joint extension was the smallest and most variable (25±9 deg), with very large extensions at all other joints (hip: 104±12 deg, knee:

Table 1. Animal and performance data for all jumps

Individual	Body mass (g)	Jump duration (ms)	Take-off angle (deg)	Left/right angle (deg)	Jump distance (cm)	Velocity ($m\ s^{-1}$)	Peak single-foot force (total BW)
1	56.0	136	29.1	5.6	69.5	2.10	2.00
		124	23.5	16.0	68.4	2.18	1.82
2	41.4	156	16.2	−42.0	48.3	1.71	1.50
		196	28.3	19.4	67.2	2.10	2.71
		212	26.0	25.7	70.0	2.22	2.46
		152	28.1	−33.1	75.0	2.31	3.89
3	82.2	104	26.1	8.4	78.4	2.36	2.48
		124	30.4	6.6	83.2	2.39	2.48
Mean±s.d.	55.3±17.8	151±37	26.0±4.5	0.8±24.8	70.0±10.4	2.17±0.22	2.42±0.72

Negative values for left/right angle are to the left. Peak single-foot forces are divided by the total body mass of the frog.
BW, body weight.

The Journal of Experimental Biology (2014) doi:10.1242/jeb.110296

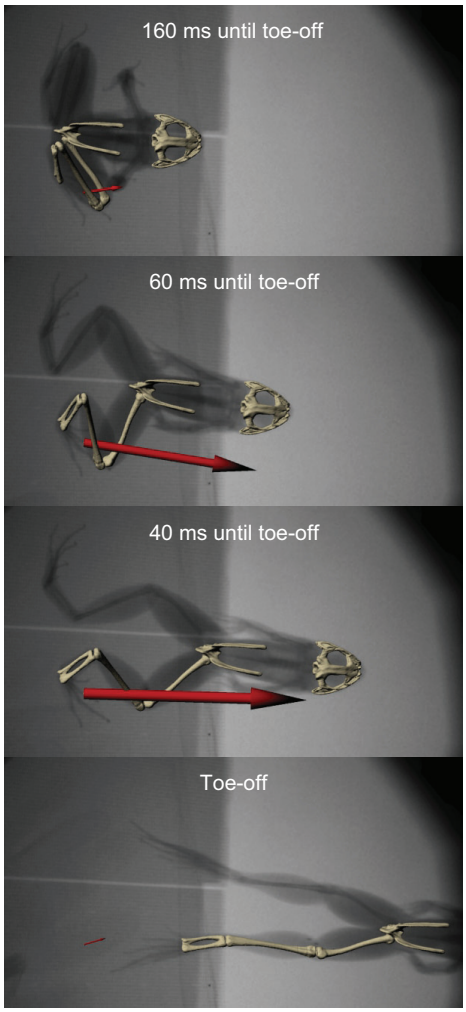

Fig. 2. Sequential X-ray video frames from the example jump, with rotoscoped bones and a scaled GRF vector. This is a postero-dorsal view, ~45 deg off vertical. See supplementary material Movie 1.

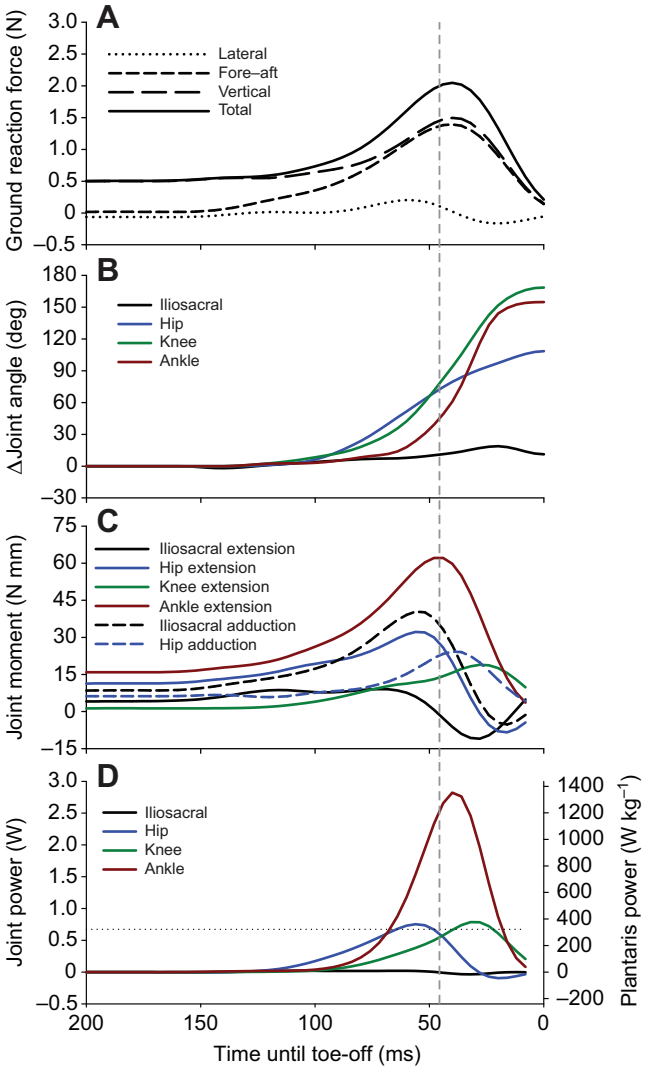

Fig. 3. Kinetics and kinematics of an example jump. The dashed gray line across all graphs represents the start of elastic recoil at the ankle joint, as determined by the timing of peak ankle moment. (A) Ground reaction forces. Positive vertical force represents an upwards reaction force, positive fore–aft force is a forwards reaction force and positive lateral force is a lateral reaction force. (B) Change in joint angle from initial position during the jump for the iliosacral, hip, knee and ankle joints in the flexion–extension axis. Positive values are extension. (C) Joint moments in the flexion–extension (all joints) and abduction–adduction axes (hip and iliosacral only). Abduction–adduction moments were low and constant at the knee and ankle, and are not shown. Positive values are extension and adduction. (D) Joint powers in the flexion–extension axis. Ankle power is also expressed in W kg^{-1} of plantaris muscle mass on the right axis. The horizontal dotted line indicates the maximum isotonic power output of the plantaris muscle.

160±11 deg, ankle: 142±8 deg) (Fig. 3B). The start of joint motion proceeded in a proximal-to-distal sequence, with the iliosacral and hip joint movement starting approximately simultaneously, followed by the knee joint and finally the ankle joint (Fig. 3B). Joint motions in the abduction/adduction axis were also typically small (<15 deg) with the exception of a single jump with an anomalous starting posture (unusually abducted hips), which showed 51 deg of hip adduction.

In distal joints (i.e. ankle and knee), joint moments were more stereotyped and dominated by a single axis than proximal joints. At the iliosacral joint, there was typically a low extension moment at rest, which increased early in the jump before decreasing and eventually becoming a flexion moment (Fig. 3C). Iliosacral adduction moment followed a similar pattern, but the magnitudes of these relative to each other varied considerably between jumps, with either predominating or both being equal (supplementary material Fig. S2). Hip moments followed a similar pattern to iliosacral flexion–extension moments, though with less variability. Hip flexion and adduction moments rose early, then decreased and, on occasion, became negative late in the jump (Fig. 3C). Hip extension moment was typically larger than hip adduction moment (Fig. 3C). Knee and ankle extension moments rose rapidly during the early jump, then decreased as the frog approached toe-off (Fig. 3C), while adduction–abduction moments were low and variable throughout the jump (supplementary material Fig. S2). All long-axis moments were low and showed little variability within each jump (supplementary material Fig. S2).

Substantial joint power was only produced in the flexion–extension axis, if at all, with the sole exception of a substantial hip adduction power for the jump with an unusual starting posture. Iliosacral extension power was always minimal compared with the other joints, rarely exceeding 0.1 W (Fig. 3D). Hip extension power was highly variable in magnitude (mean ± s.d. peak power, 0.24±0.26 W) (Fig. 3D), mostly due to high values from a single

The Journal of Experimental Biology (2014) doi:10.1242/jeb.110296

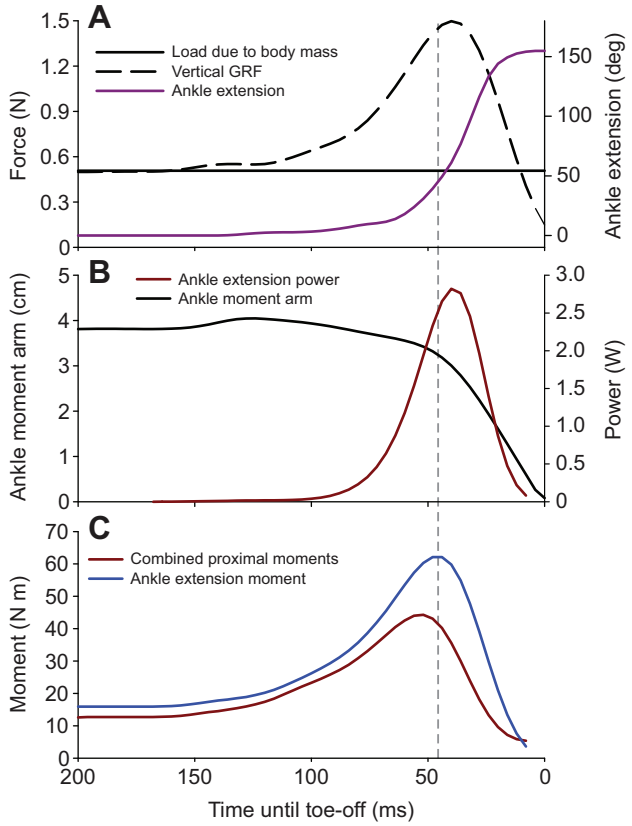

Fig. 4. Dynamic catch mechanism evaluations. The dashed gray line across all graphs represents the start of elastic recoil at the ankle joint. (A) Gravitational mechanism. Load due to body mass, vertical GRF and ankle extension over time. The vertical GRF exceeds the gravitational load long before joint movement or elastic recoil. (B) Variable mechanical advantage mechanism. External moment arm at the ankle in the flexion–extension axis and ankle extension power over time. External moment arm is high early in the jump, leading to low mechanical advantage, but decreases immediately prior to and during elastic recoil, resulting in increasing mechanical advantage. (C) Proximal joint moment mechanism. Ankle extension moment and combined proximal joint moments (summed hip and knee moments) over time. Early in the jump, ankle and proximal joint moments increase in tandem, but the combined proximal joint moments begin decreasing shortly before and throughout elastic recoil.

individual. Peak knee and ankle extension powers were both very high, but ankle power was consistently higher (knee: 0.57±0.29 W, ankle: 1.43±0.81 W) (Fig. 3D). When ankle power was normalized by dividing by the mass of a single plantaris muscle, calculations showed that ankle power per kg of plantaris muscle mass reached as high as 1352 W kg^{-1} (mean peak power of 934±311 W kg^{-1}) (Fig. 3D), often exceeding the isotonic muscle power (322 W kg^{-1}) (Roberts et al., 2011) by more than threefold. The high power observed at the ankle supports the idea that there is significant elastic energy storage and recovery at this joint. Also consistent with the idea of a power amplifying mechanism was the observation that the duration of loading (time from start of ankle moment rise to peak ankle moment) was typically more than twice the duration of recoil (time from peak ankle moment to toe-off) (2.3±0.7), with a loading duration of 117±36 ms and a recoil duration of 52±6 ms.

Mechanism tests

External moment arm (*R*) consistently started at a high value at the beginning of the jump and decreased rapidly during the period of elastic recoil. The beginning of the rapid decline in *R* occurred on average at 86±18 ms before toe-off and 33±18 ms before peak ankle moment (Fig. 4B). At the time of peak ankle moment, moment arm had only decreased by 9±10% relative to the start of the jump (Fig. 4B), but then declined to nearly zero during the period of elastic recoil.

The GRF exceeded the force due to gravity well before the peak ankle moment, and most of the increase in ankle moment occurred after the GRF passed 1 BW. Peak ankle moment occurred 56±6 ms before toe-off, but the gravitational load was surpassed by the vertical component of GRF at 135±29 ms before toe-off, and 79±28 ms before ankle elastic recoil (Fig. 4A).

To evaluate the contribution of proximal joint moments to elastic pre-loading, we calculated the sum of the hip and knee moment, as both of these will contribute to the increase in the acceleration of the body and an increase in GRF. During the early part of the jump, the summed proximal joint moments rose to 3.7±1.6 times the resting value, peaking only 14±7 ms before the beginning of elastic recoil and 70±10 ms before toe-off (Fig. 4C). At the beginning of the elastic recoil period, the summed proximal joint moments had declined to 0.88±0.10 times the maximum value, and continued to decline until shortly before toe-off (Fig. 4C). This indicates that early in the jump, as ankle moment rises during elastic loading, the force that the ankle moment must overcome to produce motion also rises substantially (Fig. 4C). Immediately before elastic recoil, there is a period during which ankle moment continues to rise, while the combined moment from the proximal joints declines, facilitating the initiation of ankle extension (Fig. 4C). Throughout the remainder of the jump, the proximal joint moments continue to decline.

DISCUSSION

Proximal joint moments and mechanical advantage as dynamic catch mechanisms

The results above suggest that proximal muscular moments and changing mechanical advantage both act to resist ankle movement during an elastic pre-loading period and allow motion during recoil, while the force of gravity alone is insufficient to oppose ankle movement during loading. Early in the jump, proximal muscular moments and a relatively poor mechanical advantage (Fig. 1C, Fig. 3, Fig. 4) function in concert to allow for high forces and to resist motion during a period of increasing moment at the ankle during elastic pre-loading. Shortly before elastic recoil begins, both the proximal muscular moments and the external moment arm decrease, allowing joint motion powered by the release of stored elastic energy.

The dynamic mechanisms favoring elastic pre-loading identified here may be applicable beyond frogs, potentially playing a role in the jumps of many tetrapod species. As in the jumps of other tetrapods, the hindlimb joints extend in proximo-distal sequence (Aerts, 1998; Bobbert and van Soest, 2001; Henry et al., 2005), which has been shown to increase the work done at each joint before take-off and allow maximal leg extension (Bobbert and van Soest, 2001). Increased proximal muscular moments will initially oppose the ankle moment, impeding joint motion and allowing elastic energy storage, before declining and thereby facilitating elastic recoil. Moment arm may also change during joint extension in other species. As the leg straightens via the extension of the joints, the joints will become closer to the overall axis of the leg from the center of mass to the ground contact point. If the GRF is parallel and near this axis, the external moment arms will decrease for all joints as the leg extends (Fig. 2). While differences in leg configuration and muscular anatomy may alter the efficacy of these mechanisms, the underlying mechanics are present in all vertebrate jumpers. This

may have facilitated the evolution of power amplification in frogs and other vertebrates by allowing them to utilize pre-existing vertebrate jump mechanics to allow greater loading of elastic tendons. Similarly, it may allow many less-specialized species to gain some limited benefit from elastic energy storage, including humans (Bobbert, 2001; Henry et al., 2005).

Dynamic catch mechanisms may not be possible in all situations, particularly if there is no GRF, as in raptorial feeding appendages or kicking limbs (Burrows and Morris, 2001; Patek et al., 2004). Without a substrate reaction force, the distal element of the joint would begin moving at any non-zero extensor torque, preventing substantial loading of the elastic element via proximal joint moments. Variable mechanical advantage may also be less effective in these systems, as the external moment arm is dictated solely by distal segment anatomy, and cannot therefore be changed dynamically by alterations to the location or orientation of the GRF. Consequently, proximal moment and variable mechanical advantage mechanisms are unlikely to be useful for prey capture or striking mechanisms involving elastic energy storage, requiring alternative mechanisms such as anatomical catch mechanisms.

Limitations of this study

Our tests for hypothesized catch mechanisms involve somewhat qualitative predictions for the timing of kinematic and kinetic events. For example, we predicted that mechanical advantage would be low during elastic pre-loading but then increase steadily during joint motion and elastic recoil. Modeling suggests that this pattern increases the total power and work output of a muscle–tendon–load system (Roberts and Marsh, 2003), but there is not yet a theoretical basis for predicting the precise pattern of mechanical advantage that would result in the best muscle–tendon performance. It is also true that while our study demonstrates that both body acceleration due to proximal muscle action and a changing mechanical advantage contribute to effective elastic energy pre-loading at the ankle, we cannot at this point determine the relative importance of these two mechanisms. Furthermore, all three mechanisms tested involve the pattern of joint moments and motions and are thus at some level interdependent, and none of them are exclusive.

Our measurements include some error due to the challenges of determining center of pressure accurately in small animals, leading to our choice of a fixed center of pressure at the centroid of the foot. While our sensitivity analysis shows that the resulting errors in measured joint moments do not likely undermine our conclusions, the absolute values of measured joint moments will be affected. Such error may explain the observation that during the period of elastic loading the measured power output sometimes exceeds the maximum power output expected for the plantaris muscle (322 W kg^{-1}) (Roberts et al., 2011). The discrepancy occurs for a period of only ~10 ms in most jumps. Transfer of power from the knee musculature to the ankle via the biarticular plantaris is unlikely to explain this discrepancy or contribute to our estimates of maximum power output at the ankle; prior work on *R. pipiens* has shown that the plantaris has no moment arm at knee extension angles of less than 100 deg (Astley and Roberts, 2012), which does not occur until 5±2 ms after ankle elastic recoil. Furthermore, in all but the two weakest jumps, peak ankle power divided by the summed plantaris and knee extensor muscle mass still exceeded peak isotonic muscle power (404±125 W kg^{-1}).

A catch mechanism by any other name?

The effect of proximal joint moments and variable mechanical advantage – opposing joint motion early in the jump and thereby allowing increased elastic energy storage – can be seen as analogous to the anatomical catch mechanisms seen in invertebrates. However, whether or not the label ‘catch mechanism’ applies to these phenomena depends upon how narrowly or broadly the term is defined. If a catch mechanism completely prevents joint motion until elastic recoil, with all subsequent motion powered purely by elastic recoil, these mechanisms fall short, as there is joint motion prior to recoil (Fig. 3) and muscle shortening during or following recoil (Roberts and Marsh, 2003; Astley and Roberts, 2012). Alternatively, if the definition of catch mechanism includes any mechanism that resists motion during the loading of the elastic structure, even the load of gravity or the inertia of the body or limb segments can function as catch mechanisms (Galantis and Woledge, 2003; Roberts and Marsh, 2003), rendering the term so common as to be trivial and uninformative.

We suggest the term ‘dynamic catch mechanisms’, defined as a change in force, moment or external lever arm that can initially impede motion during the elastic loading phase then subsequently change to allow or even enhance motion during elastic recoil. This term emphasizes that these catch mechanisms are the product of the balance of forces and moments throughout the limb during the jump, rather than the discrete anatomical structures that characterize the anatomical catch mechanisms of invertebrates. In anuran jumping, both proximal joint moments and mechanical advantage function as dynamic catch mechanisms, but it is possible that other species may use only one of these, both, or additional, unknown mechanisms to achieve catapult-like jump mechanics.

MATERIALS AND METHODS

Animals

Three adult *R. pipiens* (mean ± s.d.: snout–vent length 9.9±1.1 cm, mass 59.9±20.7 g) were obtained from a commercial supplier. The frogs were kept in an enclosure with water and land areas and fed crickets three times per week. Prior to experimental trials, frogs were anesthetized with MS-222 (Sigma-Aldrich) and metal markers (1 mm tantalum beads and 0.45 mm diameter insect pins) were implanted in the ilia, femur, tibia and fused tarsal bone to aid in rotoscoping. Beads were implanted into holes in the bone created with a hand drill, while insect pins were pushed directly into the bone at locations where drilling was not possible because of overlying fascia (anterior ilia and distal femur). Pins were inserted in the left and right anterior tips of the ilia and distal femur, while three beads were implanted in the tibia and two in the tarsal bone. Following the experiments, all frogs were euthanized with an overdose of MS-222, frozen, and scanned using X-ray computed tomography, and the muscles of the proximal hindlimb and plantaris dissected and weighed. All procedures were approved by the Brown University IACUC.

Force plate

A six-axis force transducer (Model Mini-40, ATI, Apex, NC, USA) was mounted to a custom-made housing of radiolucent material (acrylic) (supplementary material Fig. S3). The force sensor (diameter 40 mm, height 14 mm) was mounted at the lateral edge of the base (19.5×11.7×0.5 cm, sensor center offset 3.7 cm laterally from the center of the plate), to prevent it from obstructing X-rays, with the platform surface attached on top in a cantilevered position via firmly set screws into the tool face of the force sensor (supplementary material Fig. S3). A similarly sized base was constructed at the same level as the sensing platform surface and immediately adjacent to it (supplementary material Fig. S3). A high-friction substrate (drywall medium sanding screens, 3M, St Paul, MN, USA) was attached to the surface of the force plate to provide traction. Four metal beads were implanted in the force plate surface to allow it to be located relative to the bones based on X-ray video data. During jumps, frogs were placed on the middle of the structure such that the right foot and approximately half of their body rested on the force platform surface and the remainder rested upon the raised portion of the base. Jumps were discarded

if any portion of the left foot contacted the force platform surface. Forces were recorded using Igor 6.0 (WaveMetrics Inc., Lake Oswego, OR, USA) at 10 kHz, then filtered with a 15–25 Hz FIR low-pass filter with a Hanning window, with cut-off frequency selected for each jump to minimize noise without substantially altering the timing or magnitude of the forces (supplementary material Fig. S4). The start and end recording pulses from the cameras were also recorded, to allow synchronization between force and X-ray data.

The fully assembled force plate was calibrated via loading with known masses at multiple locations on the sensing plate in all three directions. Calibrations were performed before and after each day of testing, as well as at least once during the testing day. Calibrated force measurements were accurate to within 2% of actual load at all locations on the plate. No detectable displacement of the embedded beads occurred during jumps, so deflection was minimal.

X-ray Reconstruction of Moving Morphology (XROMM)

The position of limb segments, the frog's body and the force plate were determined simultaneously using XROMM, specifically via scientific rotoscoping (Brainerd et al., 2010; Gatesy et al., 2010). Two image intensifiers were positioned beneath the force plate, perpendicular to each other and at 45 deg relative to horizontal, and illuminated with X-ray emitters at 45 kVp and 200 mA. Each image intensifier was equipped with a synchronized high-speed camera (Phantom V10, Vision Research Inc., Wayne, NJ, USA) recording at 250 frames s^{-1} with an exposure time of 750 µs. The resulting X-ray videos were undistorted and calibrated using a 64-point calibration object (Brainerd et al., 2010). Frogs were positioned on the jumping platform as described above and induced to jump via sudden movements of the experimenter and gentle taps on the side of the body resting on the non-sensing section of the platform.

Frogs were euthanized, frozen with legs in an extended position, and scanned using X-ray computed tomography (slice thickness 0.625 mm, slice resolution 0.1875 mm). DICOM stacks were segmented using Amira 4.0 (Mercury Computer Systems Inc., Chelmsford, MA, USA) and OsiriX (http://www.osirix-viewer.com) to produce isolated bone models of the skull, hips, femur, tibia and tarsal bone, as well as DICOM stacks containing all tissue in the pre-sacral body, post-sacral body, thigh, shank and tarsal. A script custom-written by the authors in MATLAB 2010b (The MathWorks Inc., Natick, MA, USA) was used to calculate dimensions, mass, center of mass location and moments of inertia in all axes for each segment from these DICOM stacks, assuming a density of 1.056 g cm^{-3} for soft tissue and 1.93 g cm^{-3} for bone (Biltz and Pellegrino, 1969).

To determine the kinematics of the right leg, hips and pre-sacral body, we used scientific rotoscoping (Gatesy et al., 2010) with additional guidance from the implanted markers. Two undistorted X-ray camera views were created in Maya 2012 (Autodesk, San Rafael, CA, USA) and used to position each bone independently in the calibrated space, thereby reconstructing the three-dimensional movements of each bone and their joints. Joint coordinate systems were positioned at the approximate center of rotation for each joint, with the *x*-axis aligned with the long axis of the distal bone. For the ankle and knee joints, the flexion–extension axis (*Z*-axis) was aligned parallel to the flattening of the tarsals and tibia, respectively. At the hip, the flexion–extension axis was defined as perpendicular to the plane of curvature of the femur. Because the sacrum was too indistinct to rotoscope, the ilio-sacral joint motion was determined from the hips and skull. The center of rotation was positioned mid-way between the anterior tips of the ilia, with the flexion–extension (*Z*) axis passing through each tip of the ilia and the long axis (*X*) intersecting the occipital condyle of the skull. All joint motions were computed in the *ZYX* rotation sequence. Jump velocity and angle (horizontal and vertical) were determined from the rotoscoped skull motion at toe-off.

Inverse dynamics

To compute joint moments and powers, we used inverse dynamics software (Visual3D, C-motion, Germantown, MD, USA). Limb segment positions and motions were imported using virtual markers created in Maya at the tips of each set of joint axes, as well as a virtual marker positioned at the anterior tip of the skull and distal surface of the tarsal bone. Segment masses and rotational moments of inertia about all three axes were computed from CT scans using a custom-written MATLAB script. Force plate location in calibrated X-ray space was derived from the metal markers implanted in the plate surface. Forces were downsampled in Igor, then imported into Visual3D. For each joint, we computed motion in 6 degrees of freedom, angular velocity and acceleration, joint moment, joint force and joint power, resolved using the Cardan sequence in the coordinate system of the distal joint element. The start of joint motion in a given degree of freedom was defined as the point at which the motion reaches 5% of the maximum joint excursion. Because moment arm declined towards zero at toe-off, the start of moment arm change was defined as 95% of the maximum value.

Because of limitations in the precision of our apparatus, the center of pressure could not be accurately calculated, and was instead placed at the centroid of a polygon defined by the toe tips and lateral and medial distal corners of the tarsal bone. We performed a sensitivity analysis on the effects of center of pressure determination by placing the center of pressure at the centroid and points bordering the polygon, then comparing the effect on joint moments at all joints and in all axes. All points were within 1.5 cm of the centroid except for the tips of the extremely elongate 4th and 5th toes (2.5 and 2.1 cm, respectively); thus, the 4th and 5th toes were excluded from further sensitivity analysis. The analysis indicated that moment magnitudes will vary because of changes of center of pressure location, but the overall pattern of moment over time, particularly for crucial joints and axes in this study, remains consistent (supplementary material Fig. S5), including the timing of peak ankle extension moment (which defines the start of recoil). Our test of the gravitational mechanism will be completely insensitive to this variation, while external moment arm data will simply be increased or decreased by a fixed amount for a static center of pressure at a different location. We were unable to examine the effect of dynamic movement of the center of pressure throughout the jump, but inspection of high-speed videos of these frogs jumping showed that the foot loses contact with the ground in a proximal-to-distal 'peeling' motion following ankle extension, suggesting that center of pressure motion will be greatest at the very end of the jump, after recoil has begun. Catch mechanisms are evaluated on timing and pattern (see below), and this sensitivity analysis suggests the effect on such evaluations will be minimal.

Evaluation of proposed mechanisms for elastic pre-loading

The hypothesized mechanisms for elastic pre-loading were evaluated by examining the timing patterns of joint dynamics. Because tendons are passive elastic structures, and therefore length depends only upon force, increasing force indicates that the tendon must be stretching, and recoil may only occur when force declines. As the plantaris muscle–tendon unit has a constant moment arm at the ankle (Astley and Roberts, 2012), ankle moment is directly proportional to tension in the plantaris tendon, and thus recoil begins at the peak of ankle moment. An effective elastic pre-loading mechanism should resist motion early in the jump during elastic loading, but allow it late in the jump via elastic recoil. As such, the opposing mechanism is predicted to be in the state that acts to limit joint movement for a given ankle muscle force (e.g. low mechanical advantage, high proximal joint moments) during elastic loading in the early jump, then to transition to the state that allows joint movement (e.g. high mechanical advantage, low proximal joint moments) during the period of elastic recoil. Mechanisms that do not follow this pattern, those that reverse it, or those in which the transition occurs substantially before or after elastic recoil would be ill-suited to functioning as a catch mechanism.

To assess the role of changing mechanical advantage, we determined how the external moment arm – the distance between ankle flexion–extension axis and the GRF vector – changed over the course of the jump. The internal moment arm of the plantaris at the ankle (*r*) in the flexion–extension axis is constant throughout the range of motion (Astley and Roberts, 2012); thus, any change in mechanical advantage (*R*/*r* in Eqn 1) must be due to changes in the external moment arm, *R*. A large external moment arm will result in a poor mechanical advantage (ideal for loading the elastic tendon), while a small external moment arm will result in a mechanical advantage conducive to elastic recoil. While it is not possible to predict the precise mechanical advantage needed to allow elastic recoil, this mechanism should require a

long external moment arm (poor mechanical advantage) early in the jump, followed by a decrease during the period of elastic recoil.

To assess whether the force of gravity on the body was sufficient to allow elastic pre-loading, we determined the vertical GRF necessary to counteract the gravitational load imposed by the fraction of the frog's body supported on the force plate. If gravitational forces are sufficient to allow significant elastic loading, then elastic loading should occur prior to substantial increase in GRF, and recoil should begin when GRF exceeds the gravitational load.

To test whether muscle action at proximal joints aided in elastic pre-loading at the ankle, we first calculated the flexion/extension, abduction/adduction and long axis rotation moments at the knee and hip. The plantaris muscle is an ankle extensor, and only the components of the hip and knee moments that act in the ankle flexion/extension axis will tend to increase ankle moment and resist ankle motion. Thus, we transformed the calculated hip and knee moments into the ankle frame of reference. To determine the total effect of proximal joints on ankle moment, we calculated a summed hip and knee moment in the ankle flexion/extension axis. We predicted that this combined measure of proximal joint moments would increase early in the jump, during elastic loading, thereby increasing the effective load that the ankle must overcome (Fig. 1B), then begin to decrease immediately prior to elastic recoil.

Acknowledgements
The authors would like to thank Angela M. Horner and Erika Giblin for assistance during testing, Stephen M. Gatesy for rotoscoping assistance, and Robert Kambic, Angela M. Horner and Scott Selbie for help with Visual3D data import and processing.

Competing interests
The authors declare no competing financial interests.

Author contributions
Both authors were involved in conception, design and execution of the experiment, interpretation of the findings, and drafting and revising the article.

Funding
This work was supported by the National Science Foundation (NSF) IOS grant 642428 to T.J.R.

Supplementary material
Supplementary material available online at
http://jeb.biologists.org/lookup/suppl/doi:10.1242/jeb.110296/-/DC1

References

Aerts, P. (1998). Vertical jumping in galago senegalensis: the quest for an obligate mechanical power amplifier. *Philos. Trans. R. Soc. B* **353**, 1607-1620.
Astley, H. C. and Roberts, T. J. (2012). Evidence for a vertebrate catapult: elastic energy storage in the plantaris tendon during frog jumping. *Biol. Lett.* **8**, 386-389.
Bennet-Clark, H. C. and Lucey, E. C. A. (1967). The jump of the flea: a study of the energetics and a model of the mechanism. *J. Exp. Biol.* **47**, 59-67.
Biltz, R. M. and Pellegrino, E. D. (1969). The chemical anatomy of bone. I. A comparative study of bone composition in sixteen vertebrates. *J. Bone Joint Surg. Am.* **51**, 456-466.
Bobbert, M. F. (2001). Dependence of human squat jump performance on the series elastic compliance of the triceps surae: a simulation study. *J. Exp. Biol.* **204**, 533-542.
Bobbert, M. F. and van Ingen Schenau, G. J. (1988). Coordination in vertical jumping. *J. Biomech.* **21**, 249-262.
Bobbert, M. F. and van Soest, A. J. (2001). Why do people jump the way they do? *Exerc. Sport Sci. Rev.* **29**, 95-102.
Brainerd, E. L., Baier, D. B., Gatesy, S. M., Hedrick, T. L., Metzger, K. A., Gilbert, S. L. and Crisco, J. J. (2010). X-ray reconstruction of moving morphology (XROMM): precision, accuracy and applications in comparative biomechanics research. *J. Exp. Zool. A* **313**, 262-279.
Burrows, M. (2003). Biomechanics: froghopper insects leap to new heights. *Nature* **424**, 509.
Burrows, M. (2006). Jumping performance of froghopper insects. *J. Exp. Biol.* **209**, 4607-4621.
Burrows, M. and Morris, G. (2001). The kinematics and neural control of high-speed kicking movements in the locust. *J. Exp. Biol.* **204**, 3471-3481.
Emerson, S. B. (1978). Allometry and jumping in frogs: helping the twain to meet. *Evolution* **32**, 551-564.
Galantis, A. and Woledge, R. C. (2003). The theoretical limits to the power output of a muscle-tendon complex with inertial and gravitational loads. *Proc. R. Soc. B* **270**, 1493-1498.
Gatesy, S. M., Baier, D. B., Jenkins, F. A., Jr and Dial, K. P. (2010). Scientific rotoscoping: a morphology-based method of 3-D motion analysis and visualization. *J. Exp. Zool. A* **313**, 244-261.
Gronenberg, W. (1996). Fast actions in small animals: springs and click mechanisms. *J. Comp. Physiol. A* **178**, 727-734.
Heitler, W. J. (1974). The locust jump. *J. Comp. Physiol. A* **89**, 93-104.
Henry, H. T., Ellerby, D. J. and Marsh, R. L. (2005). Performance of guinea fowl Numida meleagris during jumping requires storage and release of elastic energy. *J. Exp. Biol.* **208**, 3293-3302.
Lutz, G. J. and Rome, L. C. (1996). Muscle function during jumping in frogs. I. Sarcomere length change, EMG pattern, and jumping performance. *Am. J. Physiol.* **271**, C563-C570.
Marsh, R. L. (1994). Jumping ability of anuran amphibians. *Adv. Vet. Sci. Comp. Med.* **38B**, 51-111.
Patek, S. N., Korff, W. L. and Caldwell, R. L. (2004). Biomechanics: deadly strike mechanism of a mantis shrimp. *Nature* **428**, 819-820.
Patek, S. N., Dudek, D. M. and Rosario, M. V. (2011). From bouncy legs to poisoned arrows: elastic movements in invertebrates. *J. Exp. Biol.* **214**, 1973-1980.
Peplowski, M. M. and Marsh, R. L. (1997). Work and power output in the hindlimb muscles of Cuban tree frogs Osteopilus septentrionalis during jumping. *J. Exp. Biol.* **200**, 2861-2870.
Roberts, T. J. and Azizi, E. (2011). Flexible mechanisms: the diverse roles of biological springs in vertebrate movement. *J. Exp. Biol.* **214**, 353-361.
Roberts, T. J. and Marsh, R. L. (2003). Probing the limits to muscle-powered accelerations: lessons from jumping bullfrogs. *J. Exp. Biol.* **206**, 2567-2580.
Roberts, T. J., Abbott, E. M. and Azizi, E. (2011). The weak link: do muscle properties determine locomotor performance in frogs? *Philos. Trans. R. Soc. B* **366**, 1488-1495.
Zug, G. R. (1978). Anuran locomotion: structure and function. II. Jumping performance of semiacquatic, terrestrial, and arboreal frogs. *Smithson. Contrib. Zool.* **276**, iii-31.

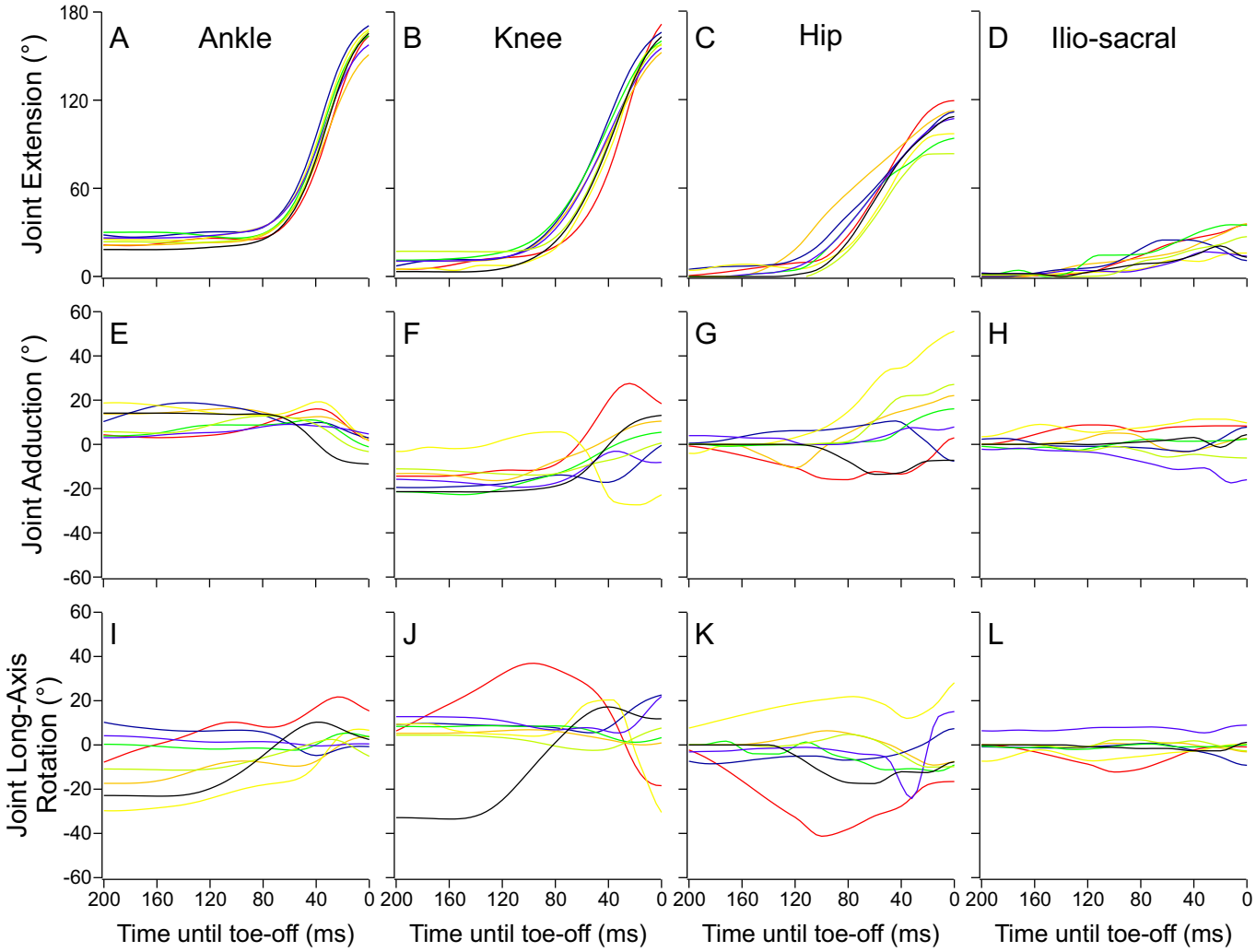

Fig. S1. All joint rotations for all individuals. Each individual is represented by a different color, with a consistent color scheme in this figure and Supplementary Figure 3. Positive values represent joint extension and adduction. A) Ankle joint flexion-extension. B) Knee joint flexion-extension. C) Hip joint flexion-extension. D) Ilio-sacral joint flexion-extension. E) Ankle joint adduction-abduction. F) Knee joint adduction-abduction. G) Hip joint adduction-abduction. H) Ilio-sacral joint adduction-abduction. I) Ankle joint long-axis rotation. J) Knee joint long-axis rotation. K) Hip joint long-axis rotation. L) Ilio-sacral joint long-axis rotation.

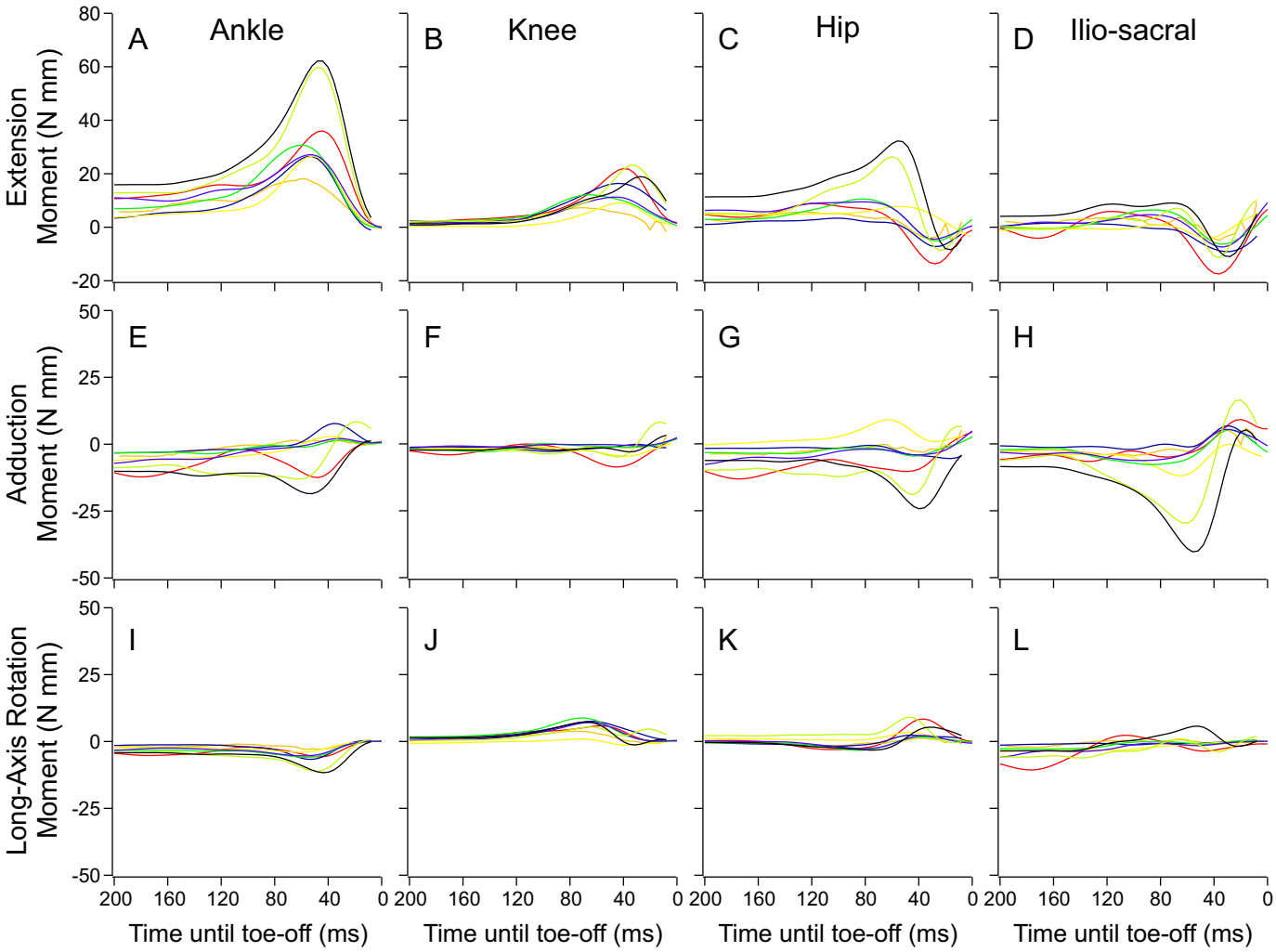

Fig. S2. All joint moments for all individuals. Each individual is represented by a different color, with a consistent color scheme in this figure and Supplementary Figure 2. A) Ankle joint extension moment. B) Knee joint extension moment. C) Hip joint extension moment. D) Ilio-sacral joint extension moment. E) Ankle joint adduction moment. F) Knee joint adduction moment. G) Hip joint adduction moment. H) Ilio-sacral joint adduction moment. I) Ankle joint long-axis rotation moment. J) Knee joint long-axis rotation moment. K) Hip joint long-axis rotation moment. L) Ilio-sacral joint long-axis rotation moment.

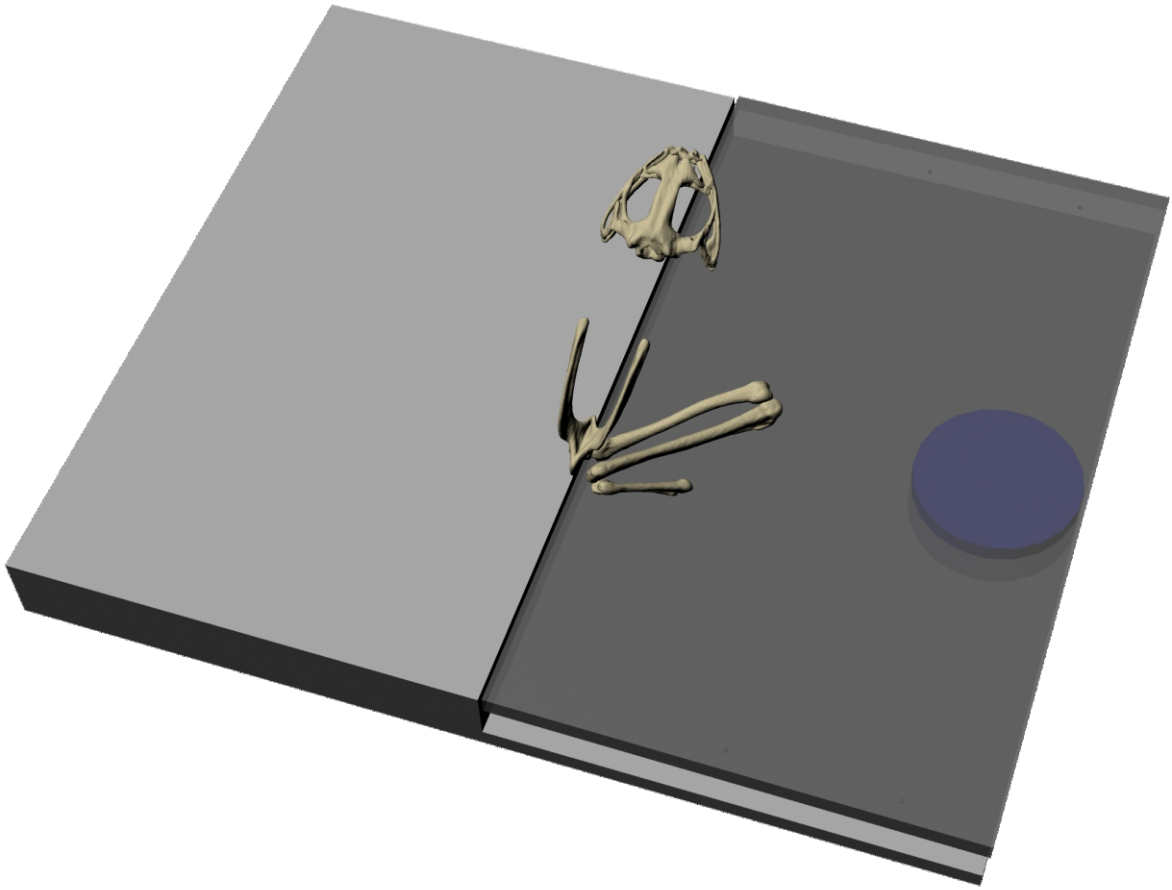

Fig. S3. Reconstruction of the force sensor and custom housing. The force sensor is the blue cylinder, the sensing portion of the platform is show in dark grey, the inert portion of the platform and base is shown in light grey. Frog bones are shown in starting posture.

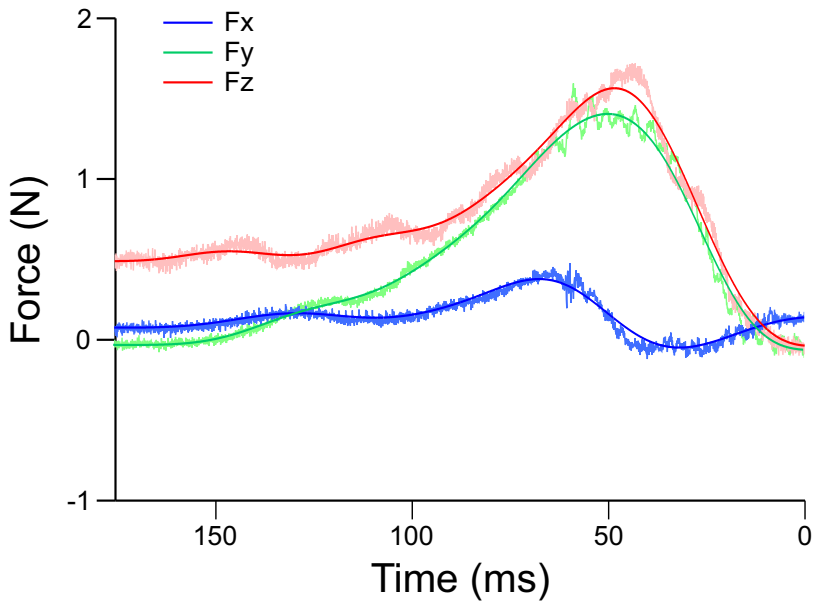

Fig. S4. The filtered and unfiltered forces recorded from the forceplate for a single jump. Pale colors are the unfiltered data and solid colors are the filtered. This jump was filtered with a 25 Hz low-pass IIR filter with a Hanning window.

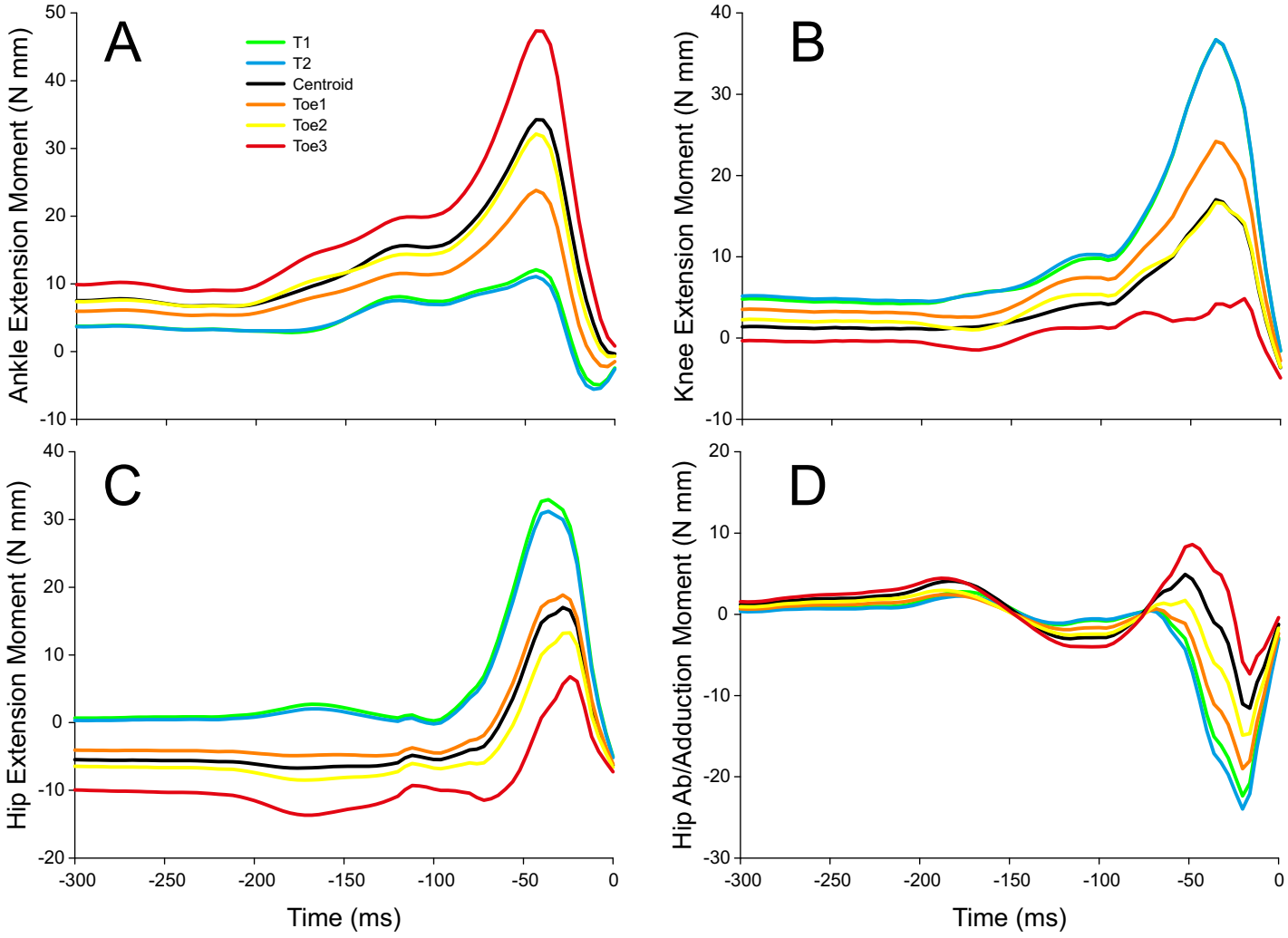

Fig. S5. Sensitivity test data. Moments are given for the same force and jump with the center of pressure located at the tips of the three shorter toes, the most lateral points of the distal tarsal (T1 & T2), and the centroid of the foot. A) Ankle extension moment. B) Knee extension moment. C) Hip extension moment. D) Hip adduction moment.

Movie 1. X-ray video of the example jump shown in Fig. 2, with rotoscoped bones and a scaled GRF vector. This is a postero-dorsal view, ~45 deg off vertical.